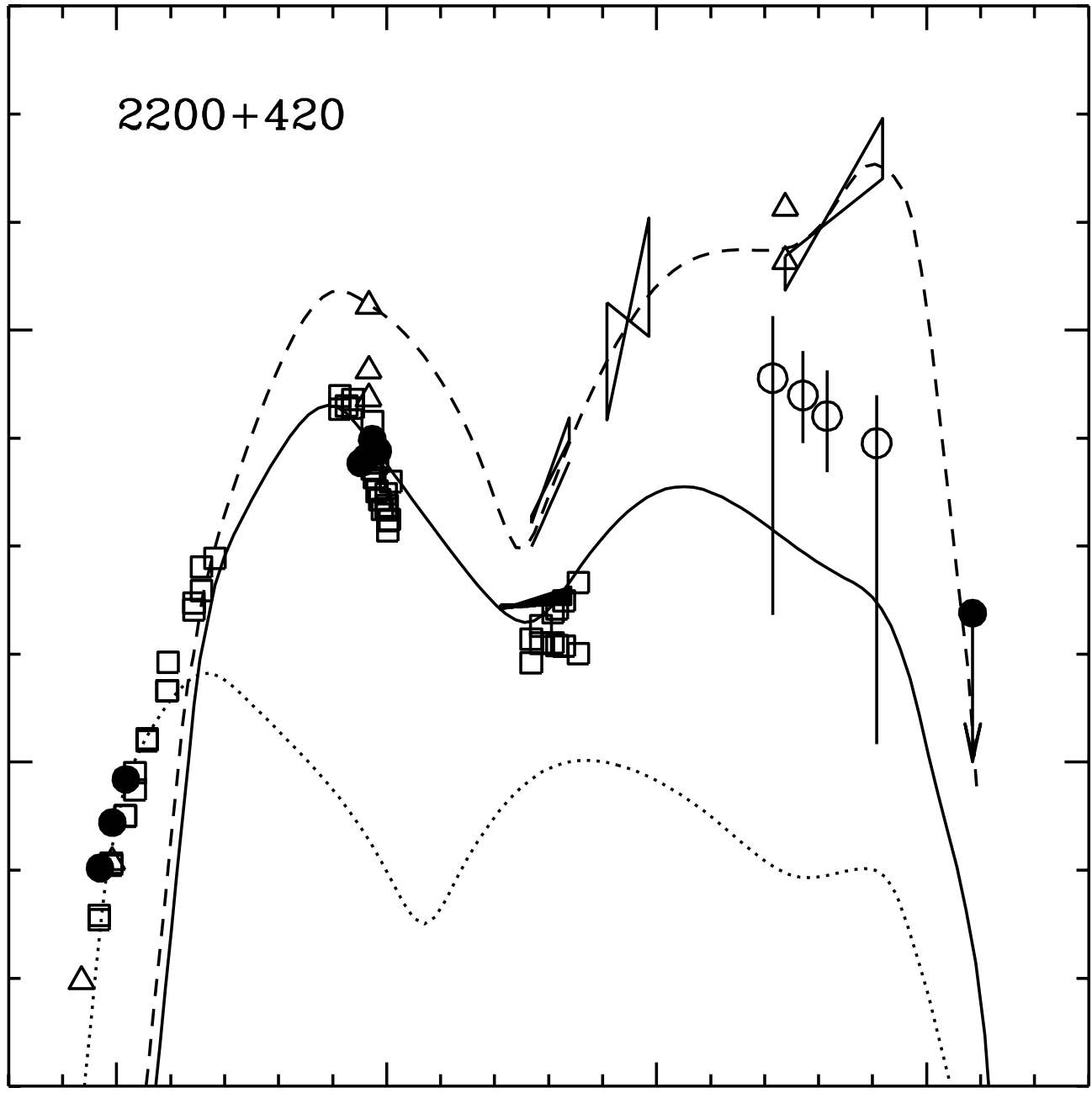


2200+420

$\text{Log } \nu F_\nu \text{ (erg cm}^{-2} \text{ s}^{-1}\text{)}$

$\text{Log } \nu \text{ (Hz)}$



**ASCA and contemporaneous ground-based observations
of the BL Lacertae objects 1749+096 and 2200+420 (BL Lac)**

Rita M. Sambruna

The Pennsylvania State University, Department of Astronomy and Astrophysics, 525
Davey Lab, State College, PA 16802

Gabriele Ghisellini

Osservatorio Astronomico di Brera, via Bianchi 46, 22055 Merate (LC), Italy

Eric Hooper

Harvard-Smithsonian Center for Astrophysics, 60 Garden St., Cambridge, MA 02138

R. I. Kollgaard

Fermi National Accelerator Laboratory, Pine Road and Kirk Street, Batavia, IL 60510

Joseph E. Pesce

The Pennsylvania State University, Department of Astronomy and Astrophysics, 525
Davey Lab, State College, PA 16802

C. Megan Urry

STScI, 3700 San Martin Dr., Baltimore 21218, MD

ABSTRACT

We present ASCA observations of the radio-selected BL Lacertae objects 1749+096 ($z=0.32$) and 2200+420 (BL Lac, $z=0.069$) performed in 1995 September and November, respectively. The ASCA spectra of both sources can be described as a first approximation by a power law with photon index $\Gamma \approx 2$. This is flatter than for most X-ray-selected BL Lacs observed with ASCA, in agreement with the predictions of current blazar unification models. While 1749+096 exhibits tentative evidence for spectral flattening at low energies, a concave continuum is detected for 2200+420: the steep low-energy component is consistent the high-energy tail of the synchrotron emission responsible for the longer wavelengths, while the harder tail at higher energies is the onset of the Compton component. The two BL Lacs were observed with ground-based telescopes from radio to TeV energies contemporaneously with ASCA. The spectral energy distributions are consistent with synchrotron-self Compton emission from a single homogeneous region shortward of the IR/optical wavelengths, with a second component in the radio domain related to a more extended emission region. For 2200+420, comparing the 1995 November state with the optical/GeV flare of 1997 July, we find that models requiring inverse Compton scattering of external photons provide a viable mechanism for the production of the highest (GeV) energies during the flare. In particular, an increase of the external radiation density and of the power injected in the jet can reproduce the flat γ -ray continuum observed in 1997 July. A directly testable prediction of this model is that the line luminosity in 2200+420 should vary shortly after (~ 1 month) a non-thermal synchrotron flare.

Subject Headings: Galaxies:active – BL Lacertae objects:individual (1749+096 and 2200+420) – Blazars: X-ray and γ -ray emission – Blazars: multifrequency variability – Radiation mechanisms: non-thermal.

1. Introduction and Motivation

Among Active Galactic Nuclei, blazars are the most dominated by non-thermal activity from a relativistic jet oriented close to the line of sight, with synchrotron emission from radio to UV/X-rays, and inverse Compton up to γ -rays (e.g., Urry & Padovani 1995; Kollgaard 1994). As such, they represent a fortuitous natural laboratory to study the

physics of the jets and, ultimately, the mechanisms of energy extraction from the central black hole, a fundamental goal of extragalactic astrophysics.

The blazar family is traditionally divided into two major subgroups, depending on the strength of the optical emission lines: in Flat Spectrum Radio Quasars (FSRQs) the lines are broad and strong (rest-frame equivalent width $EW_r \gtrsim 5 \text{ \AA}$), while in BL Lacertae objects (BL Lacs), where the lines are weak ($EW < 5 \text{ \AA}$) or absent (e.g., Stickel et al. 1991). However, the distinction into FSRQs and BL Lacs based on the optical spectra has been recently blurred by the detection of strong optical emission lines in several sources traditionally classified as BL Lacs (Scarpa & Falomo 1997), including the class prototype, 2200+420 (BL Lac; Vermeulen et al. 1995; Corbett et al. 1996), one of the targets discussed in this paper.

Blazars in existing complete samples have subtly different spectral energy distributions (SEDs) that give clues about the underlying jet physics (Sambruna, Maraschi, & Urry 1996). The SEDs are characterized by two broad spectral components, the first one extending from radio to X-rays, and interpreted as due to synchrotron radiation, and a second component from medium-hard X-rays to γ -rays (up to TeV energies), attributed to inverse Compton scattering of photons of various origins off the jet electrons (e.g., Mukherjee et al. 1997; Hartman 1996; von Montigny et al. 1995). A practical way to parameterize the different SEDs is through the radio-to-X-ray spectral index α_{rx} , which is > 0.8 in objects with the synchrotron peak in IR/optical (Low-energy peaked BL Lacs, LBLs, and FSRQs) and < 0.8 in UV/soft X-ray-peaked sources (High-energy peaked BL Lacs, HBLs; Padovani & Giommi 1995). The synchrotron and inverse Compton components peak at different locations in the SEDs depending on the bolometric jet luminosity, with a trend of decreasing peak frequency (for both spectral components) with increasing luminosity (Fossati et al. 1998; Sambruna et al. 1996).

The spectral transition from HBLs to LBLs to FSRQs can not be explained in terms of different viewing angles alone, as postulated by earlier unification schemes (e.g., Urry, Padovani, & Stickel 1991). Instead, a change of jet physical parameters is required: the higher synchrotron frequencies of HBLs suggest higher magnetic fields and/or larger electron energies than in their LBL and FSRQ counterparts (Sambruna et al. 1996; Georganopoulos & Marscher 1998). In addition, the γ -ray loudness (i.e., the ratio of the GeV to optical flux) increases from HBLs to LBLs to FSRQs, and is correlated with the luminosity of the broad lines (Sambruna 1997). This suggests that a key role for the production of the higher energies is played by the jet ambient radiation (Sambruna 1997), and indeed this hypothesis is supported by a detailed modelling of the spectral energy distributions of blazar types (Ghisellini et al. 1998). However, strong selection effects, related to the large-amplitude

variability at γ -rays combined with the limited EGRET sensitivity, could be at work at high energies exaggerating the γ -ray dominance, particularly in the more luminous quasars. More sensitive observations at GeV energies, e.g., with GLAST, will provide a crucial test of the new unification scenario at higher energies.

At lower energies, the “modified” blazar unification model is directly testable through broad-band X-ray observations. As a consequence of the synchrotron dominance, HBLs should exhibit steep and downward-curved (as a result of radiative losses) X-ray spectra, and indeed this was observed in ROSAT, EXOSAT, Ginga, and ASCA data (Kubo et al. 1998; Sambruna et al. 1997, 1994a; Perlman et al. 1996; Sembay et al. 1993). The observed 0.1–20 keV continua are typically described by a power law with photon index $\Gamma \sim 2.4$, steepening by $\Delta\Gamma \lesssim 0.5$ above a few keV. Flux and spectral variability are observed, with a trend of a harder continuum with increasing intensity (e.g., Sambruna et al. 1994b), most likely related to recent electron injection/acceleration events in the jet (Ulrich et al. 1997).

In contrast, in LBLs and FSRQs flatter X-ray spectra are predicted as a result of the larger Compton dominance. Soft X-ray observations with ROSAT and *Einstein* confirm this prediction (Sambruna 1997; Comastri et al. 1997; Urry et al. 1996; Worrall & Wilkes 1990), yielding typical slopes $\Gamma \sim 2$. Comparing the (non-simultaneous) ROSAT (0.1–2.4 keV) and *Einstein* IPC (0.3–3.5 keV) data for 13 LBLs and FSRQs, spectral upturns were inferred above ~ 1 keV in both subclasses (Sambruna 1997; Urry et al. 1996), and directly observed only in one object so far (0716+714; Makino et al. 1996). In a few LBLs the observed correlated flux-slope variability trend is in the sense of *flatter* soft X-ray spectra for *decreasing* flux, as if when the synchrotron intensity fades the flatter Compton tail is uncovered. For FSRQs, little or no flux and spectral variations (20% or less) are found from repeated ROSAT observations on timescales of days to months (Sambruna 1997), consistent with Compton dominance at X-rays in these blazars.

At hard X-rays, contrary to HBLs information has been scarce so far for LBLs. Five objects observed with EXOSAT at energies $\gtrsim 2$ keV showed rather flat spectra, $\Gamma \sim 1.5$ (Sambruna et al. 1994a,b), albeit within large errors. Ginga observations of a few sources also indicated rather flat slopes, but with a large dispersion (Ohashi et al. 1989). More observations are clearly needed to assess the continuum emission at medium-hard X-rays of LBLs and probe the modified unification model.

To this purpose, we were granted ASCA time during AO3 to observe the two sources 1749+096 ($z = 0.320$) and 2200+420=BL Lac ($z = 0.069$). Both sources belong to the complete 1 Jy sample of BL Lacs assembled at radio frequencies (Stickel et al. 1991), and can be classified as LBLs on the basis of their α_{rx} indices ($\alpha_{rx} = 0.92$ for 1749+096 and $\alpha_{rx}=0.85$ for 2200+420; Sambruna et al. 1996). They were selected because they are the

X-ray-brightest LBLs with little or no spectral information at hard X-rays. In the case of 2200+420, the comparison of the ROSAT and IPC spectra indicated an upturn of the continuum at $\gtrsim 1$ keV (Urry et al. 1996), suggesting that we might detect the Compton component with ASCA.

Another goal of our investigation is the detailed study of continuum emission processes. To this end we organized ground-base coverage at radio through optical frequencies simultaneous to ASCA for both sources. By a coincidence, 2200+420 was also observed at TeV energies with Whipple during our ASCA pointing, yielding only an upper limit on the TeV flux.

Recently, 2200+420 came into much attention since it underwent a large outburst at GeV and optical frequencies during 1997 July (Bloom et al. 1998). This LBL is also remarkable since a strong ($L_{H\alpha} \sim 10^{41}$ erg s $^{-1}$) and broad (FWHM $\sim 4,000$ km s $^{-1}$) H α emission line was detected in 1995 May-June (Corbett et al. 1996; Vermeulen et al. 1995), which appears to be variable on short (~ 1 week) timescales (Robinson 1996; Nesci & Massaro 1996). Interestingly, the line detection occurred a few months after the first EGRET detection of the source (Catanese et al. 1997). In contrast, 1749+096 was never detected in γ -rays and shows weak lines (Stickel et al. 1991).

This paper is organized as follows. The ASCA data are described in § 2, together with the results of the time and spectral analysis. We find that the 0.6–10 keV continua of both LBLs are flat ($\Gamma \sim 2.0$), with further spectral complexity over a single power law model. In the case of 2200+420, we detect a concave continuum with a hard tail emerging above 2 keV, while 1749+096 shows low-energy spectral flattening. The contemporaneous ground-based observations are presented in § 3. We construct multifrequency spectral energy distributions and compare them to published spectra (including the 1997 GeV/optical flare for 2200+420). Our results are summarized and discussed in §§ 4 and 5, with the conclusions following in § 6. Throughout this paper, $H_0=50$ km s $^{-1}$ Mpc $^{-1}$ and $q_0=0.5$ are assumed. The energy index α is defined as $F_\nu \propto \nu^{-\alpha}$.

2. ASCA Observations

2.1. Data Reduction and Analysis

We observed 1749+096 and 2200+420 with ASCA on 1995 September 22 and on 1995 November 22, respectively, for 30 ksec each. For a description of the ASCA experiment see Tanaka, Inoue, & Holt (1994). In both cases, the Solid-State Imaging Spectrometers (SIS0 and SIS1) operated in 1-CCD FAINT mode and the Gas Imaging Spectrometers (GIS2 and

GIS3) were used in Pulse-Height mode. In order to apply standard data analysis methods, the FAINT SIS mode was converted into BRIGHT2, applying the corrections for echo effect and dark frame error (see “The ASCA Data Reduction Guide”, v.2, April 1997).

The data reduction was performed using FTTOOLS v.4.0. The screening criteria for both SIS and GIS included the rejection of the data taken during the passage of the South Atlantic Anomaly and for geomagnetic cutoff rigidity lower than 6 GeV/c. We retained SIS data accumulated for Bright Earth angles $> 20^\circ$ and Elevation angles $> 10^\circ$, and GIS data accumulated for Elevation angles $> 5^\circ$. Only data corresponding to SIS grades 0, 2, 3, and 4 were accepted. Table 1 reports the effective exposures after the screening and the corresponding source count rates in the four detectors.

The source spectra and light curves were extracted from circular regions centered on the source position with radii of 4 arcmin for the SIS and 6 arcmin for the GIS, which has a larger intrinsic point spread function. In the case of the GIS we evaluated the background in circular regions of radius 4 arcmin, located about 12 arcmin away from the target where the source counts are negligible. In the case of the SIS, the background was evaluated in circular regions of radius 2 arcmin located 6 arcmin away from the target on the same chip. Since no spectral variability is apparent within the ASCA exposures, the spectra were integrated over the entire duration of the observations.

The ASCA spectra were fitted using XSPEC v.10. The SIS and GIS spectra were rebinned in order to have a minimum of 20 counts in each spectral bin to validate the use of the χ^2 statistic. In order to increase the signal-to-noise ratio we performed joint fits to the data from the 4 detectors, leaving only the normalizations as independent parameters. The 1994 May response matrices were used for the GIS spectra, while for the SIS data we used the matrices generated by the SISRMG program (v.1.1, 1997 March). The SIS and GIS data were fitted in the energy ranges 0.6–10 keV and 0.7–10 keV, where the spectral responses are best known.

2.2. Timing Analysis

The ASCA light curves of both objects were inspected for flux variability. For 1749+096 no significant flux variations were observed in either the SIS nor the GIS light curves. The χ^2 test yields a probability that the intensity is constant at $P_{\chi^2} \gtrsim 36\%$ and $\gtrsim 10\%$ for the SIS and GIS data, respectively, over a timescale of a few ($\lesssim 7$) hours.

In the case of 2200+420, flux changes were observed in the SIS0, SIS1, and GIS2 light curves, with $P_{\chi^2} \sim 1.2\%$, 0.4% , and 2% , respectively, while no variability is detected in the

GIS3 data ($P_{\chi^2} \sim 62\%$). Inspection of the light curves shows that, while the background is stable for SIS0, SIS1, and GIS3, it is variable in the case of GIS2, with $P_{\chi^2} \sim 20\%$. The largest flux variability in the light curves of SIS0, SIS1, and GIS3 is present at the beginning of the pointing: the flux increases by 25% in the first ~ 3 hours of the observation. We regard this result with caution, since instabilities in the pointing manoeuvre of the satellite could introduce spurious flux changes. In addition, P_{χ^2} appears to depend on the light curve binning, with larger probabilities for smaller binsizes (and thus lower signal-to-noise ratios). Our conclusion is that there is only tentative evidence for significant flux variability in the ASCA light curves of 2200+420.

2.3. Results of the Fits to the ASCA Spectra

The ASCA data were first fitted with a single power law absorbed at the low energies by a column density of cold gas N_H using the Morrison & McCammon (1983) cross section for photoelectric absorption, with the abundances of neutral elements other than hydrogen fixed at solar values. In the spectral fits N_H was left both free and fixed to the Galactic column density along the line of sight (see below). The results of the spectral fits are reported in Table 2 for both sources; the quoted uncertainties are the 90% confidence errors for one parameter of interest ($\Delta\chi^2=2.7$). All quantities in Table 2 are in the observer’s frame.

Figures 1 and 2 show the ASCA spectra of 1749+096 and 2200+420, together with the folded power law + Galactic N_H model (panel a), and the residuals in the form of the ratio of the data to the model (panel b). Figure 3 shows the confidence contours for the power law photon index, Γ , and the fitted column density N_H . The vertical lines mark the Galactic N_H and its nominal 90% uncertainty range.

Fits with more complex models were also attempted, as required by the data. The significance of the improvement of the fit when additional free parameters are included was evaluated using the F-test, assuming as a threshold probability for a significant improvement $P_{F=95\%}$.

2.3.1. 1749+096

The Galactic column density in the direction to 1749+096 is $N_H^{Gal} = (9.6 \pm 1.0) \times 10^{20}$ cm^{-2} (Stark et al. 1992), where the uncertainty corresponds to the 90% confidence level (Elvis et al. 1989). The ASCA data are well fitted by a single power law with N_H fixed to

the Galactic value (Table 2); the fitted slope is rather flat, $\Gamma \sim 1.8$, i.e., rising in energy emitted per decade (νF_ν). Figure 1 shows the ASCA data with the best-fit folded model (top) and the ratio of the data to the model (bottom).

However, a better fit is obtained when the column density is allowed to vary ($\Delta\chi^2=13.2$ for one additional free parameter). The fitted column density, $N_H = 1.6_{-0.34}^{+0.40} \times 10^{21} \text{ cm}^{-2}$, is larger than Galactic at $\sim 98\%$ confidence (Fig. 3), indicating excess N_H along the line of sight. While excess N_H could be at least in part due to a systematic effect of the SIS (Dotani et al. 1996), two short ROSAT PSPC observations of the source also indicated excess column densities, albeit within large uncertainties (Urry et al. 1996). Alternatively, the spectral flattening at soft energies could be due to either a convex continuum or an absorption feature.

Fitting the ASCA data with a power law plus Galactic N_H plus an absorption edge gives a formally good fit, with reduced χ^2 of $\chi_r^2=0.87$ for 615 degrees of freedom, highly improved over the single power law ($\Delta\chi^2=20$ for two additional parameters, significant at $P_F \gtrsim 99\%$). The fitted edge energy and optical depth are $E=0.73_{-0.53}^{+0.09} \text{ keV}$ and $\tau = 0.42_{-0.22}^{+0.28}$, respectively. The edge best-fit energy is consistent with the L-edge of FeIV(0.943 keV) or FeV(0.973 keV) in the rest-frame of the source (assuming $z=0.32$), or, alternatively, with the K-edge of OVIII (0.871 keV) from an intervening absorber at $z = 0.19$. However, the edge energy is poorly determined and its 90% lower limit is well below the ASCA sensitivity range. This more likely suggests that the edge is just a parameterization of low-energy spectral flattening due, for example, to an intrinsically curved continuum. Fitting the ASCA data with a broken power law model with fixed Galactic column density yields a highly improved ($P_F \gtrsim 99\%$) fit with respect to the single power law with both fixed and free N_H . A convex continuum, with steepening $\Delta\Gamma \equiv \Gamma_2 - \Gamma_1 \sim 0.4$ above $E_0=2.2 \text{ keV}$, is indicated (Table 2).

Our ASCA data represent the first observations of 1749+096 at medium-hard X-rays. Previously, the source was observed at soft energies with the *Einstein* IPC (Worrall & Wilkes 1990) and with the ROSAT PSPC (Urry et al. 1996) during an intensity state lower than ASCA in 0.5–2 keV. In both cases, the spectral parameters are poorly constrained and are consistent with ASCA within the large uncertainties.

In summary, the ASCA spectrum of 1749+096 is consistent with a hard ($\Gamma \sim 1.8$) power law. Tentative evidence for low-energy spectral flattening, which can be described either with a single power law with $\Gamma \sim 1.9$ and excess cold absorption over Galactic by $\Delta N_H \sim 7 \times 10^{20} \text{ cm}^{-2}$, or by a convex broken power law with steepening $\Delta\Gamma \sim 0.4$ above 2 keV.

2.3.2. 2200+420

Since 2200+420 is at low Galactic latitudes ($b^{\text{II}}=-10.43$), the Galactic column density of neutral hydrogen from 21 cm measurements in its direction is quite high, $(2.02 \pm 0.01) \times 10^{21} \text{ cm}^{-2}$ (Elvis et al. 1989). In addition, the source is located behind a molecular cloud from which CO emission and absorption has been detected (Bania, Marscher, & Barvainis 1991; Marscher, Bania, & Wang 1991; Lucas & Liszt 1993). From recent estimates, the equivalent atomic hydrogen column density of the CO cloud is $N_H \approx 1.6 \times 10^{21} \text{ cm}^{-2}$ (Lucas & Liszt 1993). Thus, the total Galactic column density in the direction to 2200+420 (atomic + molecular) is $\approx 3.6 \times 10^{21} \text{ cm}^{-2}$.

As apparent from Table 2, the fit with fixed Galactic absorption is acceptable, $\chi_r^2=0.97/798$. Inspection of the residuals in Figure 2 shows, however, the presence of excess flux below $\sim 1 \text{ keV}$, suggesting a concave spectrum. Leaving the N_H free to vary yields a significantly better fit ($P_F \gtrsim 99\%$), with column densities in the range $2.3\text{--}3.0 \times 10^{21} \text{ cm}^{-2}$ (Fig. 3). The fitted N_H is lower than the total Galactic column density, suggesting a concave continuum. Alternatively, if the ASCA-fitted column density represents the total true value of the Galactic N_H along the line of sight, a contribution from the molecular cloud of $N_H \sim 7 \times 10^{20} \text{ cm}^{-2}$ is inferred, lower than current estimates (Lucas & Liszt 1993).

We next fitted the 0.6–10 keV data with a broken power law with total Galactic N_H fixed to $3.6 \times 10^{21} \text{ cm}^{-2}$. The fit with this model is highly improved ($\Delta\chi^2=45$ for two additional parameters, $P_F > 99\%$) with respect to the fit with the single power law and Galactic column density, and even with respect to the power law with free N_H ($\Delta\chi^2=9$ for 1 additional parameter, $P_F \gtrsim 99\%$). The fit yields a low-energy photon index $\Gamma_1 \sim 2.3$ and a harder slope $\Gamma_2 \sim 2$ above $\sim 2 \text{ keV}$ (Table 2). We interpret the steep component at $\lesssim 2 \text{ keV}$ as the high-energy end of the synchrotron emission responsible for the longer wavelength emission (§ 3.2.2), while the flatter tail at higher X-ray energies is the onset of the Compton component extending to γ -rays.

Our ASCA data confirm for the first time the previous inference, based on non-simultaneous ROSAT and IPC data, that the X-ray continuum of 2200+420 has an upturn at \sim a few keV (Urry et al. 1996). 2200+420 was also observed at energies $\gtrsim 1 \text{ keV}$ with the *Einstein* MPC and Ginga (Bregman et al. 1990; Kawai et al. 1991), when the flux was slightly lower than ASCA (factor 1.7). The MPC slope is consistent with ASCA, while the two Ginga observations, separated by one month, yield a harder ($\Gamma \sim 1.7$) and a steeper ($\Gamma \sim 2.2$) continuum, respectively. A discussion of correlated flux-spectral variability is hampered by the different energy ranges of the various satellites; in general, a variability trend of flatter-when-fainter is apparent. However, observations with RXTE and ASCA during the flare of 1997 July, when the flux was a factor 3 higher than in 1995 November,

show a flatter ($\Gamma \sim 1.4$) continuum up to 200 keV (Madejski, Jaffe, & Sikora 1997; Makino et al. 1997), contrary to this trend.

There is mounting evidence for the presence of intrinsic absorption in the X-ray spectra of BL Lacs, at energies consistent with absorption by ionized oxygen and with column densities as low as $\tau \sim 0.2$ (Sambruna & Mushotzky 1998; Sambruna et al. 1997). We checked the ASCA data of 2200+420, which has a low redshift ($z=0.069$), for the presence of ionized oxygen absorption by adding an edge with an energy constrained to vary in the range of OVI to OVIII, i.e., 0.63–0.81 keV in the observer’s frame. No statistically significant improvement was obtained, with a formal upper limit to the optical depth of the edge of oxygen (in any ionization state) of $\tau < 1.3$ at 90% confidence.

In summary, the ASCA observations of 2200+420 in 1995 November are best-fitted by a concave broken power law with a steep photon index ($\Gamma \sim 2.3$) below 2 keV, attributed to the synchrotron emission, and a flatter tail ($\Gamma \sim 2$) at harder energies, related to the inverse Compton component. This is the first time that both spectral components are detected in the X-ray spectrum of 2200+420.

3. Observations Contemporaneous to ASCA

3.1. Radio

The Very Large Array was used to observe 1749+096 and 2200+420 in late 1995, with core radio fluxes being measured at five frequencies during each session. Table 3A reports the log of the radio observations. The observations of 1749+096 were made while the VLA was in transition from the A to B-configurations, and all of the 2200+420 data were taken in the latter configuration. The data were analyzed in the standard manner using the NRAO’s Astronomical Image Processing System (AIPS). The initial calibration was made using either 3C286 or 3C48 as the primary flux standard. Data were recorded in two 50 MHz bandpasses at each frequency, and analyzed simultaneously using the AIPS tasks IMAGR and CALIB for deconvolution and self-calibration, respectively. Two iterative cycles of IMAGR and CALIB were used for each data set, with corrections applied only to the source phases in order to preserve the absolute flux density scale.

The resulting images show no extended emission around the unresolved cores of either source, and therefore the measured flux densities were not affected by the changing resolution of the VLA. The rms error on each image was less than 1%, and the errors in the flux density are dominated by uncertainties in the overall flux calibration. We estimate these errors to be a few percent at the lower frequencies, and $\sim 5\%$ at 22 GHz. A larger

uncertainty is expected from the two observations that used 3C48 as the primary calibrator (1749+096 on 1995 September 28 and 1995 December 5) because of difficulties in obtaining an adequate calibrator solution. The 1995 November 28 observations of 2200+420 were marred by corrupted data which rendered all primary calibrator sources unuseable. Our estimates of the flux density for these data are based on the raw, uncalibrated data which should have a flux scale approximately 10% of the true scale. We have therefore increased our error estimate for the flux densities measured under these circumstances. The radio flux densities are reported in Table 3A.

3.2. Optical

3.2.1. Observations and Data analysis

Both BL Lac objects were observed at optical wavelengths in the Fall of 1995 in conjunction with the ASCA observations. CCD images in V and R were obtained for 1749+096 on the night of UT September 23, and two months later 2200+420 was imaged in $BVRI$ on UT November 23. All data were collected with the 61" reflector on Mt. Bigelow, Arizona. Only three measurements were made of 1749+096, but 2200+420 was monitored over a span of five hours. No variability was detected, and so the magnitudes were averaged over each night. Aperture photometry and growth curve analysis were performed with Stetson's (1987, 1990) DAOPHOT and DAOGROW programs.

Stray light contaminated the images on both nights, introducing spatially and temporally variable additive features. The additive nature of this light was confirmed by examining the observed magnitudes of calibrated stars in globular clusters (Christian et al. 1985; Odewahn et al. 1992) which filled the field of view of the CCD camera. Each BL Lac field contains several stars that have been calibrated to facilitate the monitoring of the AGNs (Craine, Johnson, & Tapia 1975; Smith et al. 1985; Fiorucci & Tosti 1996). In the present case, these calibration stars were used to check the validity of the data reduction and to estimate the uncertainties of the derived magnitudes. Both nights were photometric, so the external globular cluster calibrators were used to establish the transformation from instrumental to standard magnitudes. The derived magnitudes of the calibrated field stars were consistent with the values in the literature for 1749+096 and about 0.05 mag fainter for 2200+420. (The calibrated values for the latter object have systematic differences of up to 0.1 mag; see Fiorucci & Tosti 1996.) The flux values of 2200+420 were made brighter by 0.05 mag to compensate. Both sets of calibration stars have an rms scatter of ≈ 0.1 mag about the values given in the literature; 0.1 mag was taken to be the uncertainty in the flux measurements of the program objects.

The observed magnitudes are listed in Table 3B. The second entry in the Table lists the corresponding intrinsic flux densities, obtained after dereddening the magnitudes with $A_V=0.7$ for 1749+096 and $A_V=1.2$ for 2200+420. The extinction values were calculated following the law of Cardelli, Clayton, & Mathis (1989), assuming $R_V=3.1$ (the latter value, however, is uncertain and could be as high as 5). For 1749+096, A_V was derived from the ASCA-fitted N_H (in the conservative assumption that spectral bending is due to excess absorption) and using the conversion $A_V = 4.5 \times 10^{-22} N_H \text{ mag cm}^2$ (Ryter 1996); the derived value, $A_V=0.7$, is 43% higher than derived from Galactic N_H only, $A_V=0.4$. For 2200+420, a similar calculation using total Galactic $N_H = 3.6 \times 10^{21} \text{ cm}^{-2}$ gives $A_V = 1.6$; fitting an optical spectrum of the source, Vermeulen et al. (1995) find that a lower value $A_V=0.9$ provides excellent results, with *a posteriori* consistency arguments. We used $A_V = 1.2$ as an intermediate value. The flux density errors listed in Table 3B include only the photometric imprecisions, with no contributions from ill-determined uncertainties in the extinction parameters. The effects of variations in the extinction values were explored in calculations of optical spectral indices.

3.2.2. Optical indices and α_{ox} indices

We calculated optical energy indices α_{opt} from a linear fit to the dereddened flux densities, in order to compare α_{opt} with the ASCA slope and gain insights about the origin of the X-rays. For 2200+420, a spectral index of $\alpha_{opt} = 0.76 + / - 0.20$ was derived assuming the fluxes in Table 3B which were dereddened using $A_V = 1.2$ and $R_V=3.1$ (see above). This value of α_{opt} is slightly flatter than the ASCA slope measured between 0.6–2 keV, $\alpha_{X,soft} = 1.31 \pm 0.08$ (Table 2), indicating that further steepening could be occurring between the optical and the X-ray bands, in agreement with synchrotron emission where radiative losses are responsible for depleting the emission at the higher energies first. However, the optical slope is sensitive to the adopted reddening. Increasing R_V to the rather high value of 5 or lowering A_V to 0.9 both produced $\alpha_{opt} \sim 1.1$, consistent with the ASCA slope, while higher extinction, $A_V = 1.6$, flattened the slope to $\alpha_{opt} \sim 0.31$, again flatter than the X-ray slope.

For 1749+096, we obtain $\alpha_{opt} = 0.08 + / - 1.2$ from the two optical measurements in Table 3B, very poorly constrained due to the large uncertainty of the V magnitude and the small wavelength difference between the V and R bands. Altering A_V and R_V had negligible effect compared to the error on α_{opt} .

The composite spectral index, α_{ox} , connecting the optical and X-rays (defined between $5.5 \times 10^{14} \text{ Hz}$ and 1 keV), turns out to be less dependent on the reddening and thus a more

reliable indicator of the synchrotron slope above the optical peak. For 2200+420, using the optical V flux in Table 3B and the 1 keV X-ray flux in Table 2 we derive $\alpha_{ox} = 1.29 \pm 0.02$, in excellent agreement with $\alpha_{X,soft}$. Using the optical fluxes dereddened with $A_V=1.6$ and $A_V = 0.9$ we obtain $\alpha_{ox} = 1.24 \pm 0.02$ and $\alpha_{ox} = 1.35 \pm 0.02$, consistent within the errors with $\alpha_{X,soft}$. We thus conclude that the similarity of the optical-to-X-ray and soft X-ray (0.5–2 keV) slopes provides support for our earlier claim that the steep power law component detected in the ASCA data of 2200+420 is the high-energy tail of the synchrotron component responsible for the lower energies.

For 1749+096, we derive $\alpha_{ox} = 1.36 \pm 0.05$, steeper than the ASCA slope, using the optical flux in Table 3B. Using the optical flux dereddened with a lower $A_V = 0.4$, we obtain $\alpha_{ox} = 1.32 \pm 0.05$, again steeper than ASCA. This indicates that the X-rays belong to a different spectral component than the lower frequencies, most likely the onset of a Compton scattering component.

3.3. γ -rays

By a fortunate coincidence, 2200+420 was observed at TeV energies with the Whipple Observatory between 1995 October 17 and November 25, overlapping with our ASCA pointing. Only an upper limit of 5.3×10^{-10} photons $\text{cm}^{-2} \text{s}^{-1}$ for to the flux above 350 GeV was obtained (Catanese et al. 1997). At GeV energies, 2200+420 was first detected with EGRET in 1995 January–February, ~ 9 months before the ASCA and Whipple observations, with a significance of 4.4σ (Catanese et al. 1997). A large flare at GeV energies was later detected in 1997 July (Bloom et al. 1998); the flux was a factor ~ 4 higher than the 1995, with a flare of amplitude 60% in ~ 8 hrs. The EGRET spectrum was significantly flatter during the flare, $\Gamma = 1.68 \pm 0.12$, than during the lower level of early 1995, when $\Gamma = 2.27 \pm 0.30$ (Bloom et al. 1998). This confirms the trend of harder γ -ray spectra with increasing luminosity which has also been observed in other γ -ray blazars (Mukherjee et al. 1997).

3.4. Multifrequency Spectral Energy Distributions

The radio to γ -ray spectral energy distributions (SEDs) of 1749+096 and 2200+420 from our contemporaneous ASCA and ground-based observations are shown in Figures 4 and 5, respectively. For 1749+096, which was never detected at γ -rays, the plotted upper limit to the GeV flux is equal to the EGRET sensitivity threshold. Plotted with different

symbols are also SEDs derived from published data for both sources. For 1749+096, we plotted non-simultaneous literature data, representing an “average” spectral distribution. For 2200+420, the SEDs from the 1988 campaign (Bregman et al. 1990; Kawai et al. 1991) and from the 1997 GeV/optical outburst (Bloom et al. 1998; Madejski et al. 1997; Makino et al. 1997) are shown. The optical datapoints were dereddened using $A_V=0.7$ for 1749+096 and $A_V=1.2$ for 2200+420 (§ 3.2.1).

As expected (see § 1), the radio to X-ray flux distributions of both sources peak at low frequencies, below the X-ray regime. Following Sambruna et al. (1996), we performed a parabolic fit to the radio through optical/X-ray 1995 SEDs of both sources (filled symbols) to determine the value of the peak frequency, ν_p , as discussed in detail in Appendix 1. We obtain $\nu_p = 1.4 \times 10^{13}$ Hz for 1749+096 and $\nu_p = 2.2 \times 10^{14}$ Hz for 2200+420, comparable to the values derived by Sambruna et al. (1996) based on literature data. The same fits yield an estimate of the luminosity at the peak frequency, L_p , and of the integrated radio-to-X-ray synchrotron luminosity, L_{sync} : for 1749+096, $L_p = 1.6 \times 10^{33}$ erg s $^{-1}$ Hz $^{-1}$ and $L_{sync} = 1.1 \times 10^{47}$ erg s $^{-1}$, for 2200+420 $L_p = 4 \times 10^{29}$ erg s $^{-1}$ Hz $^{-1}$ and $L_{sync} = 3 \times 10^{44}$ erg s $^{-1}$. Uncertainties are 35% for L_{sync} , 30% for L_p , and 10% for ν_p (Appendix 1).

In the case of 2200+420, comparison of the “quiescent” 1995 state with the 1997 flare shows that large flux and spectral variability occurred above a few keV. The X-ray flux increased by a factor 3 and hardened from $\Gamma \sim 2.0$ to $\Gamma \sim 1.4$. A similar behavior of hardening of the spectrum with increasing intensity is also observed in the EGRET band when the 1995 January and the 1997 July EGRET spectra are compared. Moreover, the flatter 1997 γ -ray spectrum suggests a second peak in the Compton component at $\gtrsim 10^{24}$ Hz in addition to the peak around 10^{22} Hz.

In the case of 1749+096, the 1995 SED corresponds to a high state in optical and X-rays with respect to historical spectra. The ASCA data lie above the extrapolation of the lower frequencies (§ 3.2.2), indicating that a second spectral component must be present in the SED, although at a level currently under the EGRET sensitivity limit (arrow in Figure 4). We will return to the spectral distributions of the two sources in § 5.2.

4. Summary of the Observational Results

We have presented ASCA and contemporaneous radio through γ -ray observations of the two LBLs 1749+096 and 2200+420 (=BL Lac). Our principal observational results are summarized as follows:

- The ASCA spectra of 1749+096 and 2200+420 can be described by single power laws

with photon indices $\Gamma \sim 1.8$ and $\Gamma \sim 2.1$, respectively.

- 1749+096 exhibits tentative evidence for spectral flattening at low energies. A convex broken power law, with steepening $\Delta\Gamma = 0.4$ above 2.2 keV, provides a good fit to the data. Alternatively, there is excess absorption by cold gas ($\Delta N_H \sim 7 \times 10^{20} \text{ cm}^{-2}$) along the line of sight.
- There is evidence for a concave spectrum in 2200+420, with a steep component ($\Gamma \sim 2.3$) below ~ 2 keV and a harder tail ($\Gamma \sim 2$) at higher energies.
- Contemporaneous radio to optical measurements confirm that the spectral energy distribution of both sources peak at $\sim 10^{13-14}$ Hz, as expected since they are LBLs.
- During the 1997 July GeV/optical flare, the X-ray continuum of 2200+420 flattened dramatically with respect to our “quiescent” state of 1995 November. The γ -ray spectrum was flatter than during 1995 January.

5. Discussion

5.1. ASCA Spectra of Blazars: Implications for the Unification Models

In its operational lifetime, ASCA has observed up to now several blazars of the HBL, LBL, and FSRQ types. A subset of objects observed simultaneously with EGRET, including 7 HBLs, 4 LBLs, and 7 FSRQs, is presented in Kubo et al. (1998). We add the two LBLs studied here, 1749+096 and 2200+420, and three FSRQs with published ASCA data, 0836+71 and 0438–436 (Cappi et al. 1997), and PKS 1510–089 (Singh, Shrader, & George 1997).

The ASCA spectra of the FSRQ subgroup are generally well described by a single power law model; the fitted photon indices span the range $\Gamma = 1.3 - 1.8$ and have mean $\langle\Gamma_{FSRQ}\rangle = 1.59$ and dispersion $\sigma_{FSRQ}=0.14$. The ASCA spectra of HBLs are to a first approximation described by a single power law with slopes in the range $\Gamma = 2.0 - 2.7$, with mean $\langle\Gamma_{HBL}\rangle = 2.47$ and dispersion $\sigma_{HBL} = 0.36$. In contrast, for LBLs Γ is in the range 1.6–2.1, with $\langle\Gamma_{LBL}\rangle = 1.85$ and $\sigma_{LBL} = 0.16$. Our tentative conclusion, based on limited statistics, is that ASCA observations of blazars confirm the expectations of the modified unification models (§ 1): while HBLs have in general steep hard X-ray continua, dominated by the synchrotron high-energy tail, LBLs and FSRQs are characterized by flatter slopes, as expected if the inverse Compton component becomes dominant (but see below for FSRQs). Clearly, in order to draw definitive conclusions larger, possibly complete, samples

are needed, especially of LBLs, which we anticipate from the public archives within the next few years.

Indeed, in the LBLs 2200+420 and 0716+714, which are both GeV sources, the synchrotron and inverse Compton component are explicitly resolved at X-rays: in both cases the ASCA spectra are best-fitted by a concave broken power law, with a steep power law at softer energies and a flat tail emerging above ~ 2 keV (Table 2 and Makino et al. 1996, respectively). Similarly, ROSAT observations contemporaneous to ASCA for another GeV-bright LBL, 0235+164, are consistent with a steeper component in a range of softer energies (Madejski et al. 1996). It is interesting that the α_{rx} indices of these three LBLs are in the range 0.75–0.85, i.e., close to the dividing line between HBLs and LBLs; they could thus be “transitional” cases, which would explain their concave X-ray spectra as a mix of synchrotron and inverse Compton.

The ASCA data for FSRQs are consistent with flat X-ray continua, at the hard end of the distribution for the blazar class. However, it is important to realize that the FSRQs so far observed with ASCA are either at large redshifts, $z > 1$, and/or are strong GeV γ -ray emitters (e.g., Thompson et al. 1995). Given the anticorrelation between the X-ray slope and z (e.g., Sambruna 1997), and the fact that GeV blazars are dominated at higher energies by a hard Compton tail, there is a clear bias for flat X-ray slopes for the current ASCA sample of FSRQs. Thus the results for FSRQs are still inconclusive for what concerns blazar unified models; a clearer test will come from medium-hard X-ray observations of low- z (non-GeV) FSRQs. Indeed, our study of the ROSAT pointed spectra of a large (41 objects) sample of FSRQs (with $z=0-3$) already shows that these sources have a wide distribution of soft X-ray slopes, $0.5 \lesssim \Gamma \lesssim 2.5$, indistinguishable from LBLs and with a large overlap with HBLs at matching redshifts (Sambruna 1997; see also Padovani, Giommi, & Fiore 1997). This suggests the existence of a subclass of steep soft X-ray FSRQs with possibly unusual intrinsic conditions. Moreover, our recent deep X-ray survey of blazars (Wide Angle ROSAT Pointed Survey; Perlman et al. 1998) is finding more and more examples of FSRQs with HBL-like spectral distributions; this new FSRQ subclass represents a sizable fraction (25%) of the total FSRQ population. It will be important to study with ASCA and SAX their hard ($\gtrsim 2$ keV) X-ray continua to verify whether their high-energy continua are steep and convex, as for HBLs, or whether a flat component arises, similar to LBLs and high- z FSRQs, and to determine the true origin of the soft X-ray flux (non-thermal synchrotron from the jet versus thermal emission from the disk). Multifrequency observations of these “HBL-like” FSRQs are also needed to study in detail the continuum emission processes and clarify the role of this new blazar class for the unified models.

5.2. Interpretation of the SEDs of 1749+096 and 2200+420

5.2.1. General Considerations

While there is consensus that the smooth, variable, and polarized radio-to-UV emission from blazars is due to synchrotron emission from high-energy electrons in relativistic motion (e.g., Angel & Stockman 1980; Blandford & Rees 1978), the detailed mechanisms for the production of the high-energy continuum are still unclear. The X-ray to γ -ray continuum is generally attributed to inverse Compton (IC) scattering of either the synchrotron photons themselves (synchrotron-self Compton, SSC; Maraschi, Ghisellini, & Celotti 1992) or ambient thermal radiation from the accretion disk and/or the Broad Line Regions (External Compton, EC; Sikora, Begelman & Rees 1994; Dermer & Schlickeiser 1993; Ghisellini & Madau 1996).

However, irrespective of the origin of the seed photons, the synchrotron plus IC interpretation implies that there must be close correspondence between the synchrotron and inverse Compton portions of the spectrum, since both are produced by the same electron population. For a one-zone, homogeneous model where a population of relativistic electrons, distributed as a broken power law with break energy γ_{peak} , emits synchrotron radiation with a peak at ν_S , the corresponding peak of the IC flux must be at $\nu_{SSC} \propto \gamma_{\text{peak}}^2 \nu_S$ for the SSC process, or $\nu_{EC} \propto \gamma_{\text{peak}}^2 \Gamma \nu_0$ for the EC case (where Γ is the bulk Lorentz factor, and ν_0 the frequency where the external radiation peaks). Moreover, variability of the synchrotron flux should be accompanied by variability of the corresponding IC flux; the amplitude of the latter is different in the various models (e.g., Ulrich et al. 1997) and can be used in principle to put constraints on the origin of the seed photons. Inspection of Figure 5 shows that, at least in the case of 2200+420 where the data coverage is better, the SED exhibits two broad peaks, one at $\sim 10^{14}$ Hz (§ 3.4), which we identify with the synchrotron component, and a second one between 100 MeV and a few GeV, which can be attributed to the inverse Compton component.

From the data in Figure 5, it is possible to derive an order of magnitude for the magnetic field, B (in Gauss), and the electron energy γ_{peak} , for both the SSC and EC models (where δ is the beaming factor):

$$(\gamma_{\text{peak}}^{SSC})^2 = \frac{3\nu_C}{4\nu_S} \quad (1)$$

$$B^{SSC} = \frac{1+z}{\delta} \frac{\nu_S^2}{2.8 \times 10^6 \nu_C} \quad (2)$$

$$(\gamma_{\text{peak}}^{EC})^2 = \frac{3\nu_C}{4\nu_0} \frac{1+z}{\delta\Gamma} \quad (3)$$

$$B^{EC} = \frac{\Gamma\nu_S\nu_0}{2.8 \times 10^6\nu_C} \quad (4)$$

(e.g., Sambruna et al. 1997 and references therein). As an example we now apply these relations to the 1997 SED of 2200+420, which is the best constrained. If we set, from Figure 5, $\nu_S = 10^{14}$ Hz and $\nu_C = 10^{24}$ Hz, we derive $\gamma_{\text{peak}}^{SSC} \sim 9 \times 10^4$ and $B^{SSC} = 3.8 \times 10^{-3}/\delta$ Gauss. Within the SSC scenario, the ratio L_C/L_S between the γ -ray and the optical synchrotron luminosity is equal to the ratio between the synchrotron and the magnetic energy density. Setting $L_C/L_S \sim 3$ from Figure 5 and measuring the size through the variability time-scale, $R \sim ct_{\text{var}}\delta$, in the SSC case we obtain:

$$t_{\text{var}} \sim \left(\frac{2L_S}{3c^3\delta^6 B^2} \right)^{1/2} \sim 4.8 \times 10^3 L_{S,44} \delta^{-2} \text{ days} \quad (5)$$

where $L_{S,44}$ is the observed synchrotron luminosity in units of 10^{44} erg s^{-1} . The above relation shows that the SSC model has difficulties in explaining spectra where the ratio ν_c/ν_s is large (like in the 1997 July SED of 2200+420), since in this case the resulting small magnetic field implies very large regions and/or implausibly large values of the Doppler factor: a variability timescale of ~ 1 day implies, from Eq. (5), $\delta \sim 70$.

The recent detection of a broad and variable H α emission line in 2200+420 (see § 1) may provide an argument in favor of the EC model. Application of Eqs. (3) and (4) for the EC model (assuming $\nu_0 = 10^{15}$ Hz) gives a larger magnetic field, $B^{EC} = 0.036 \Gamma$ Gauss, than the SSC model, implying the electrons at the synchrotron peak are less energetic, $\gamma_{\text{peak}}^{EC} = 2.7 \times 10^4/(\Gamma\delta)^{1/2}$. In this case the ratio L_C/L_S is controlled by the ratio of the external radiation energy density, U'_{ext} (as seen in the synchrotron-emitting blob comoving frame), and the magnetic energy density. If the external radiation is produced by the broad lines, then $U'_{\text{ext}} \sim L_{BLR}\Gamma^2/(4\pi R_{BLR}^2 c)$, where L_{BLR} is the luminosity of the broad line region of size R_{BLR} . To produce $L_c/L_S \sim 3$, we must have

$$L_{BLR} \sim \frac{3R_{BLR}^2 B^2 c}{2\Gamma^2} \quad (6)$$

which gives $L_{BLR} \sim 1.3 \times 10^{41}$ erg s^{-1} for $R_{BLR} = 5 \times 10^{16}$ cm (e.g., Dietrich et al. 1998; Ulrich et al. 1997), and for the same values as above for ν_0 , ν_c and ν_S . This value is close to the emission line luminosity seen in May and June 1995 (Vermeulen et al. 1995). Note

also that there may be other contributions to the external radiation field, coming by the accretion disk, by the intra-cloud material that scatters radiation coming from the accretion disk, and by a small portion of the broad line region illuminated by the jet.

For the 1995 SED, assuming $\nu_S = 10^{14}$ Hz, $\nu_C = 10^{22}$ Hz (as indicated by the non-simultaneous EGRET spectrum), we obtain higher magnetic fields and lower electron energies for both SSC and EC.

5.2.2. *Fits to the SEDs with Homogeneous Models*

We fitted the SEDs of 1749+096 and 2200+420 with a one-zone homogeneous model, assuming that the radio through UV emission is synchrotron radiation from a relativistic electron population and that the high-energy continuum is produced by upscattering off the same electrons of photons either internal (SSC) or external (EC) to the jet. Since the IR to UV/X-ray synchrotron emission is optically thin, these energies could be produced in a single homogeneous region. An additional spatial component, identified with different jet regions with different self-absorption turnovers, is assumed to emit the radio through submm portion of the spectra.

The external radiation is assumed to be narrowly distributed around a typical frequency $\nu_0 \approx 10^{15}$ Hz. The emission region is uniformly filled with a plasma of electrons of random energy γ and constant bulk motion with Lorentz factor Γ in a constant magnetic field B . The electrons are continuously injected at a rate $Q(\gamma) \propto \gamma^{-s}$ between minimum and maximum energies γ_{min} and γ_{max} . The steady particle distribution is computed self-consistently considering radiative cooling (including the effects of the Klein-Nishina cross-section) and electron-positron pair production. The latter effect is however unimportant given the very small intrinsic compactness (the luminosity to size ratio).

Table 4 lists the parameters assumed to reproduce the 1995 quiescent state and the 1997 flare state of 2200+420, and the 1995 SED of 1749+096, including the parameters of the radio-to-submm emitting region (labelled “Large” in Table 4). The solutions are plotted on the data in Figures 4 and 5. Our contemporaneous 1995 SEDs are underconstrained at the higher energies, where no measurements at GeV energies are available. For 2200+420, the non-contemporaneous 1995 January EGRET spectrum was used to set an upper limit to the power at GeV energies during 1995 November.

1749+096

The SED of 1749+096 can be fitted by the SSC model without any contribution from external radiation. However, the EGRET upper limit does not constrain the high energy part of the SED well enough to draw any strong conclusion. Note that the synchrotron emission peaks at relatively low frequencies, implying small values of γ_{peak} . This in turn implies that the second order Compton process is not completely inhibited by Klein-Nishina effects, and can dominate the emission at the highest frequencies (see Fig. 4), while the spectrum in the ASCA band corresponds, in the fit shown in Figure 4, to the peak of the first order Compton process.

Because of the spectral correspondence implied by the synchrotron plus IC model, in the SED in Figure 4 the soft X-rays are produced by the same electrons emitting the radio-submm energies. The IC emission of these electrons, as can be seen by the SSC fit in Figure 4, may not be negligible in the soft X-ray band during low states of the source, diluting any fast variability at these energies, consistent with the absence of flux variability in our ASCA SIS data.

2200+420

For 2200+420, the lower state of 1995 is obtained assuming that an intrinsic power of the relativistic electrons $L'_{\text{inj}} = 1.3 \times 10^{41}$ erg s⁻¹ is injected within a region of size $R = 7 \times 10^{15}$ cm. This corresponds to an intrinsic compactness $\ell_{\text{inj}} = 6.7 \times 10^{-4}$, to be compared to the compactness of external radiation, as seen in the comoving frame of the blob, of $\ell_{\text{ext}} = 2 \times 10^{-5}$. In this case the locally produced synchrotron radiation dominates the Compton cooling, and all but the highest frequencies are produced by the SSC process.

In contrast, the flaring state of the summer of 1997 can be fitted assuming that the external radiation field increased by two orders of magnitudes, providing the main contributor of seed photons at relatively high (UV) energies. As a consequence, the EC process dominates at energies larger than a few MeV, producing a flat spectrum. On the other hands, the SSC mechanism is still predominant in the X-ray range (see Fig. 5). The intrinsic injected power, in this case, has been increased by a factor 15 with respect to the value of 1995.

Note that, in principle, one can increase the ratio between the external and the synchrotron radiation by increasing Γ , since $U'_{\text{ext}} \propto \Gamma^2$, while the synchrotron radiation energy density $U'_{\text{syn}} \propto L_{\text{syn}} \delta^{-4}$. Assuming a constant broad line emission, the 100-fold increase in U'_{ext} can be achieved by a 10-fold increase in Γ , which implies an enormous change in the bulk properties of the jet.

We conclude that the flaring state of 1997 has been produced by the increase of both

the amount of the external radiation and the power injected in the jet. Together with the observational evidence of varying emission line luminosity in 2200+420, this implies that the power channeled in the jet and the ionizing radiation are linked together. If any synchrotron (and inverse Compton) flare is linked to an increase of the ionizing luminosity coming from the accretion disk, then the enhanced emission lines are best observable soon after the end of the non-thermal flare, since the time-scale of the broad line variability is of the order of $R_{\text{BLR}}/c \sim 1$ month, which can be significantly longer than the non-thermal flare. This prediction is easily testable observationally even in the absence of GeV data, by monitoring both the line and non-thermal continuum luminosity.

There is tentative evidence for a possible time lag between the 1997 July optical and GeV flares (Bloom et al. 1998), with the shorter wavelengths leading the longer ones by a few hours. Such a lag, if true, would represent a difficulty for both SSC and EC models, since in both cases one would naively expect that the synchrotron flare should anticipate the inverse Compton activity (unless some fine-tuning of the parameters is invoked in both cases). However, the sparse sampling of the data prevents any firm statement about the lag. Correlated flux variability is potentially very powerful in putting constraints to the current emission models; more intense and regular monitoring of 2200+420 at both optical and GeV energies is needed before reaching any conclusions.

6. Conclusions

Our ASCA observations of two LBLs demonstrate the importance of the X-ray band to test current unification models for blazars. This is because the synchrotron and inverse Compton components, whose balance regulates the HBLs/LBLs/FSRQs transition, cross in the X-rays; observations in this spectral region can thus directly quantify the relative importance of the two emission mechanisms in different blazar classes. Indeed, together with published data for more blazars, our ASCA observations support the current understanding that HBLs are synchrotron-dominated, while LBLs and FSRQs are Compton-dominated. Broad-band X-ray observations of larger and possibly complete samples are needed to put stronger constraints. In particular, we need to explore the X-ray and multifrequency continua of low-redshift, non-GeV FSRQs which are currently underrepresented in the ASCA and SAX archives.

Multifrequency spectral and flux variability is an essential test to probe detailed emission mechanisms for the higher energies, and assess the central question of the origin of the seed photons for the inverse Compton scattering. Our results supports current claims that External Compton scattering could be the dominant cooling mechanisms for

blazars with strong emission lines. Future monitorings of correlated line and synchrotron continuum variability have the potential to put interesting constraints on these models. In particular, an accurate estimate of the size of the Broad Line Regions in blazars is sought, since this is a fundamental parameter to calculate the radiation densities of the gas in which the relativistic jets are embedded.

RMS was funded through NASA contract NAS-38252. EJH acknowledges financial support from NASA grant NGT-51152, a NASA Graduate Student Researchers Program Fellowship at the University of Arizona, and NAGW-4266, plus observing help from John and Marcia Hooper. RIK acknowledges support by Fermi National Accelerator Laboratory under US Department of Energy contract No. DE-ACO2-76CH03000. This work was supported in part by NASA grant NAG5-2538.

7. Appendix: Parabolic fits to the radio-to-X-ray data

This section illustrates the parabolic fits to the radio-to-X-ray spectral energy distributions of 1749+096 and 2200+420 referred to in § 3.4. The data in the $\log(\nu L_\nu)$ vs. $\log \nu$ space were fitted with a function of the type

$$y = ax^2 + bx + c \tag{7}$$

following Sambruna et al. (1996). In the case of 2200+420, the fit included the softer X-rays (0.6 – 2 keV) since we have evidence that the latter are the high-energy tail of the IR/optical synchrotron emission; on the other hands, in 1749+096 the X-rays are a different emission component and were not included in the parabolic fit.

The fitted parameters are: for 1749+096, $a = -0.2476 \pm 0.0005$, $b = 6.5070 \pm 0.0046$, and $c = 3.5803 \pm 0.0142$, and for 2200+420, $a = -0.0979 \pm 0.0002$, $b = 2.8076 \pm 0.0029$, and $c = 23.3717 \pm 0.0416$. The fitted curves are shown superposed to the data in Figure A1. The derived peak frequencies ν_p , peak luminosity L_p , and total integrated luminosity L_{sync} reported in § 3.4 have uncertainties 10% (on ν_p) and 35% or less (on the luminosities); the errors were obtained by calculating the ranges of values allowed by the errors on the parabola parameters a , b , and c .

Formally, the reduced χ^2 s of the fits are high (> 2) and not acceptable; they are mostly contributed to by a few datapoints in the IR/optical regimes in both cases, which have small errorbars. More complex spectral functions are probably needed to describe the

data more closely; however, given the sparse sampling (especially in the region where the peak frequency falls, $\approx 10^{13-14}$ Hz), the parabolic function provides the simplest and yet relatively accurate approximation, useful to derive an order-of-magnitude estimate on ν_p , L_p , and L_{sync} .

REFERENCES

- Angel, J.R.P. & Stockman, H.S., *ARA&A*, 18, 321;
- Bania, T.M., Marscher, A.P., & Barvainis, R. 1991, *AJ*, 101, 2147
- Blandford, R.D. & Rees, M.J. 1978, in Pittsburgh Conference on BL Lac Objects, Pittsburgh, PA, April 24–26, 1978, Ed. A.M.Wolfe, Univ. Pittsburgh Press, p.328
- Bloom, S.D. et al. 1998, *ApJ*, in press
- Bregman, J. et al. 1990, *ApJ*, 352, 574
- Cappi, M., Matsuoka, M., Comastri, A., Brinkmann, W., Elvis, M., Palumbo, G.G.C., & Vignali, C. 1997, *ApJ*, 478, 492
- Cardelli, J.A., Clayton, G.C., & Mathis, J.S. 1989, *ApJ*, 345, 245
- Catanese, M. et al. 1997, *ApJ*, 480, 562
- Christian, C.A., Adams, M., Barnes, J.V., Hayes, D.S., Siegel, M., Butcher, H., & Mould, J.R. 1985, *PASP*, 97, 363
- Comastri, A., Fossati, G., Ghisellini, G., & Molendi, S. 1997, *ApJ*, 480, 534
- Corbett, E.A., Robinson, A., Axon, D.J., Hough, J.H., Jeffries, R.D., Thurston, M.R. & Young, S. 1996, *MNRAS*, 281, 737
- Craine, E. R., Johnson, K., & Tapia, S. 1975, *PASP*, 87, 123
- Dermer, C.D. & Schlickeiser, R. 1993, *ApJ*, 416, 458
- Dietrich, M. et al. 1998, *ApJS*, 115, 185
- Dotani, T. et al. 1996, *ASCA News No.* 4, 3
- Elvis, M., Lockman, F.J., & Wilkes, B.J. 1989, *AJ*, 97, 777
- Fiorucci, M. & Tosti, G. 1996, *A&AS*, 116, 403
- Fossati, G., Maraschi, L., Celotti, A., Comastri, A., & Ghisellini, G. 1998, *MNRAS*, 299, 433
- Georganopoulos, M. & Marscher, A. 1998, *astro-ph/9806170*
- Ghisellini, G. et al. 1998, *astro-ph/9804103*
- Ghisellini, G. & Madau, P. 1996, *MNRAS*, 280, 67
- Hartman, R. 1996, in *Blazar Continuum Variability*, Proc. of an International Workshop held in Miami, FL, 1996 February 4–7, Eds. H.R.Miller, J.R.Webb, and J.C.Noble, *Astronomical Society of the Pacific Conference Series*, Vol.110, p.333
- Kawai, N. et al. 1991, *ApJ*, 382, 508

- Kollgaard, R.I. 1994, in *Vistas in Astronomy*, 38, 29
- Kubo, H., Takahashi, T., Madejski, G., Tashiro, M., Makino, F., Inoue, S., & Takahara, F. 1998, *ApJ*, 504, 693
- Lucas, R. & Liszt, H.S. 1993, *A&A*, 276, L33
- Madejski, G., Jaffe, T., & Sikora, M. 1997, *IAU Circ.* 6705
- Madejski, G., Takahashi, T., Tashiro, M., Kubo, H., Hartman, R., Kallman, T., & Sikora, M. 1996, *ApJ*, 459, 156
- Makino, F., Mattox, J., Takahashi, T., & Kataoka, J. 1997, *IAU Circ.* 6708
- Makino et al. 1996, *MPE Rep.* 263, 413
- Maraschi, L., Ghisellini, G., & Celotti, A. 1992, *ApJ*, 397, L5
- Marscher, A.P., Bania, T.M., & Wang, Z. 1991, *ApJ*, 371, L77
- Morrison, R. & McCammon, D. 1983, *ApJ*, 270, 119
- Mukherjee, R. et al. 1997, *ApJ*, 490, 116
- Nesci, R. & Massaro, E. 1996, *IAU Circ.* 6457
- Odehahn, S. C., Stockwell, E. B., Pennington, R. L., Humphreys, R. M., & Zumach, W. A. 1992, *AJ*, 103, 3180
- Padovani, P. & Giommi, P. 1995, *ApJ*, 444, 567
- Padovani, P., Giommi, P., & Fiore, F. 1997, *MNRAS*, 284, 569
- Perlman, E.S. et al. 1998, *AJ*, 115, 1253
- Perlman, E.S., Stocke, J.T., Wang, Q.D., & Morris, S.L. 1996, *ApJ*, 456, 451
- Robinson, A. 1996, *IAU Circ.* 6443
- Ryter, C.E. 1996, *Astrophys. & Sp. Sci.*, 236, 285
- Sambruna, R.M. 1997, *ApJ*, 487, 536
- Sambruna, R.M., Barr, P., Giommi, P., Maraschi, L., Tagliaferri, G., & Treves, A. 1994a, *ApJS*, 95, 371
- Sambruna, R.M., Barr, P., Giommi, P., Maraschi, L., Tagliaferri, G., & Treves, A. 1994b, *ApJ*, 434, 468
- Sambruna, R.M., George, I.M., Madejski, G., Urry, C.M., Turner, T.J., Weaver, K.A., Maraschi, L., & Treves, A. 1997, *ApJ*, 483, 774
- Sambruna, R.M., Maraschi, L., & Urry, C.M. 1996, *ApJ*, 463, 444
- Sambruna, R.M. & Mushotzky, R.F. 1998, *ApJ*, 502, 630

- Scarpa, R. & Falomo, R. 1997, *A&A*, 325, 109
- Sembay, S., Warwick, R.S., Urry, C.M., Sokoloski, J., George, I.M., Makino, F., Ohashi, T., & Tashiro, M. 1993, *ApJ*, 404, 112
- Sikora, M., Begelman, M.C., & Rees, M.J. 1994, *ApJ*, 421, 153
- Singh, K.P., Shrader, C.R., & George, I.M. 1997, *ApJ*, 491, 515
- Smith, P. S., Balonek, T. J., Heckert, P. A., Elston, R., & Schmidt, G. D. 1985, *AJ*, 90, 1184
- Stark, A.A., Gammie, C.F., Wilson, R.W., Bally, J., Linke, R.A., Heiles, C., & Hurwitz, M. 1992, *ApJS*, 79, 77
- Stetson, P. B. 1987, *PASP*, 99, 191
- Stetson, P. B. 1990, *PASP*, 102, 932
- Stickel, M., Fried, J.W., Kuhr, H., Padovani, P., & Urry, C.M. 1991, *ApJ*, 374, 431
- Tanaka, Y., Inoue, H., & Holt, S.S. 1994, *PASJ*, 46, L37
- Thompson, D.J. et al. 1995, *ApJS*, 101, 259
- Ulrich, M.-H., Maraschi, L., & Urry, C.M. 1997, *ARAA*, 445, 502
- Urry, C.M., Padovani, P., & Stickel, M. 1991, *ApJ*, 382, 501
- Urry, C.M. & Padovani, P. 1995, *PASP*, 107, 803
- Urry, C.M., Sambruna, R.M., Worrall, D.M., Kollgaard, R.I., Feigelson, E.D., Perlman, E.S., & Stocke, J. 1996, *ApJ*, 463, 424
- Vermeulen, R.C. et al. 1995, *ApJ*, 452, L5
- von Montigny, C. et al. 1995, *ApJ*, 440, 525
- Worrall, D.M. & Wilkes, B.J. 1990, *ApJ*, 360, 396

Figure Captions

- Figure 1: ASCA spectrum of 1749+096 in 1995 September. *(a)*: Data and folded model, a single power law with photon index $\Gamma = 1.8$ plus Galactic column density; *(b)*: Residuals, plotted as the ratio of the data to the model. Data from all the four detectors, which were fitted together, are plotted in the Figure. The model provides an acceptable description of the ASCA data.
- Figure 2: ASCA spectrum of 2200+420 in 1995 November. *(a)*: Data and folded model, consisting of a single power law plus total (atomic + molecular) Galactic column density; *(b)*: Residuals, plotted as the ratio of the data to the model. Data from all the four detectors, which were fitted together, are plotted in the Figure. The model clearly underestimates the flux at the lower energies (see also Figure 3).
- Figure 3: Confidence contours for the column density N_H and the photon index from the fits to the ASCA spectra of 1749+096 and 2200+420. The 68%, 90%, and 99% confidence levels for two interesting parameters are shown. The solid lines mark the Galactic N_H in the direction to the sources (total atomic + molecular column for 2200+420); the dashed lines for 1749+096 are the formal 90% uncertainties. No range for the total Galactic column is reported for 2200+420, since the uncertainties on the molecular contribution are not known. For 1749+096, excess column density over Galactic is present at $\sim 98\%$ confidence, while in the case of 2200+420 the fitted column density is lower than Galactic, providing evidence for soft excess in this source.
- Figure 4: Multifrequency spectral energy distributions of 1749+096. The filled symbols are the ASCA data and the contemporaneous radio and optical observations obtained by us in 1995 September, while the open symbols are non-simultaneous literature data (see Sambruna et al. 1996 for references), including two ROSAT observations (Urry et al. 1996). The source was not detected at GeV energies; the arrow marks the EGRET sensitivity threshold. Plotted as a solid line is the best-fit to the 1995 data with a homogeneous, one-zone synchrotron-self Compton model; the dashed line is the contribution to the radio spectrum from a more extended region (parameters are reported in Table 4).
- Figure 5: Multifrequency spectral energy distributions of 2200+420. The filled symbols are our ASCA data and contemporaneous radio and optical observations in 1995 November, together with the TeV upper limit measured in the same period (Catanese et al. 1997). The open circles are the EGRET spectrum measured in

1995 January (Catanese et al. 1997). Plotted with triangles and open “bow-ties” in X-rays and γ -rays are the simultaneous data during the optical/GeV flare in 1997 July (Bloom et al. 1998; Madejski et al. 1997; Makino et al. 1997). The squares are the data from the 1988 multifrequency campaign (Bregman et al. 1990; Kawai et al. 1991). The solid line is the best-fit to the 1995 data with a homogeneous, one-zone synchrotron-self Compton model, while the dotted line is the contribution to the radio spectrum from a more extended region (parameters are reported in Table 4). During the “quiescent” state of 1995 November, the SSC process is primarily responsible for the production of the flux from radio to X-rays. In contrast, the flaring state of 1997 July requires an increase of the external radiation density and the power injected in the jet (Table 4), resulting in the dominance of the EC process at energies larger than a few MeV, while the SSC process still dominates the power output at X-rays and longer wavelengths. This model is plotted with a dashed line in the Figure.

- Figure A1: Contemporaneous spectral energy distributions from radio to X-rays of 1749+096 and 2200+420 in 1995. The dotted lines are the fits with a simple parabolic function (see Appendix). For 2200+420 the soft X-rays (0.6 – 2 keV) were included in the fit, as the spectral slope in this energy range is consistent with the extrapolation from the optical. For 1749+096 the X-rays were excluded from the parabolic fit since they originate through a different emission mechanism than the lower frequencies. The synchrotron peak frequency in both sources falls in a poorly sampled spectral region ($\approx 10^{13-14}$ Hz). The fitted parabola parameters (see Appendix) were used to calculate the peak frequencies, peak luminosities, and the total integrated synchrotron luminosity (§ 3.4).

Table 1: ASCA observations

Detector	Date	Start Time (UT)	Exposure ^a (s)	Count rate ^b (cts s ⁻¹)
1749+096				
SIS0	1995 Sep 22	10:34	26645	0.115 ± 0.024
SIS1			26363	0.089 ± 0.020
GIS2			28883	0.067 ± 0.002
GIS3			28891	0.093 ± 0.022
2200+420				
SIS0	1995 Nov 22	01:12	27059	0.313 ± 0.004
SIS1			26997	0.254 ± 0.003
GIS2			27665	0.176 ± 0.003
GIS3			27665	0.227 ± 0.003

Notes: a=Net exposure after data screening; b=Source net count rates in 0.6–10 keV (SIS) and 0.7–10 keV (GIS).

Table 2: Fits to the ASCA data

Model	N_H ($\times 10^{21}$ cm $^{-2}$)	Γ_1	Γ_2	E_0 (keV)	$\chi_r^2/\text{d.o.f.}$	$F_{1 \text{ keV}}$ (μJy)	$F_{2-10 \text{ keV}}^a$ ($\times 10^{-12}$ ergs cm $^{-2}$ s $^{-1}$)
1749+096							
P.Law	0.96 ^b	1.79 ± 0.04	0.89/617
	$1.64^{+0.40}_{-0.34}$	$1.89^{+0.08}_{-0.06}$	0.87/616	$0.76^{+0.05}_{-0.07}$	$3.3^{+0.6}_{-0.4}$
Broken P.law	0.96 ^b	$1.61^{+0.08}_{-0.09}$	$2.00^{+0.12}_{-0.11}$	$2.20^{+0.40}_{-0.65}$	0.86/615
2200+420							
P.Law	3.6 ^c	2.08 ± 0.03	0.97/798
	$2.71^{+0.24}_{-0.20}$	1.96 ± 0.04	0.93/797	2.22 ± 0.12	8.9 ± 0.7
Broken p.law	3.6 ^c	2.31 ± 0.08	1.97 ± 0.04	$1.78^{+0.18}_{-0.20}$	0.92/796

Notes: a=Observed fluxes (not corrected for absorption); b=Galactic column density in the direction to 1749+096, fixed; c=Total atomic and molecular column density in the direction to 2200+420 (see text), fixed.

Table 3A: Radio VLA observations

Date	Flux densities (Jy)				
	1.465 GHz	4.89 GHz	8.42 GHz	14.96 GHz	22.49 GHz
1749+096					
1995 Sep 11	0.99 ± 0.03	2.59 ± 0.08	3.89 ± 0.12	4.84 ± 0.15	6.14 ± 0.31
1995 Sep 21	1.08 ± 0.03	2.51 ± 0.08	3.85 ± 0.12	5.05 ± 0.15	...
1995 Sep 28	1.06 ± 0.05	2.47 ± 0.12	3.75 ± 0.19	5.26 ± 0.26	6.02 ± 0.42
1995 Oct 7	1.03 ± 0.03	2.54 ± 0.08	4.05 ± 0.12	5.78 ± 0.17	7.16 ± 0.36
1995 Dec 5	1.01 ± 0.05	2.52 ± 0.13	4.20 ± 0.21	5.28 ± 0.26	4.25 ± 0.30
2200+420					
1995 Nov 28	...	6.61 ± 0.66	6.25 ± 0.63	5.54 ± 0.55	...
1995 Dec 5	4.89 ± 0.24	5.97 ± 0.30	6.29 ± 0.31	5.87 ± 0.29	5.37 ± 0.38
1995 Dec 22	5.33 ± 0.16	6.34 ± 0.19	6.55 ± 0.20	5.81 ± 0.17	5.18 ± 0.26

Table 3B: Optical observations

Date	Observed Magnitudes/Intrinsic Flux densities (mJy)			
	<i>B</i>	<i>V</i>	<i>R</i>	<i>I</i>
1749+096				
1995 Sep 23	...	15.90 ± 0.30	15.43 ± 0.10	...
	...	3.05 ± 0.84	3.11 ± 0.29	...
2200+420				
1995 Nov 23	16.70 ± 0.10	15.72 ± 0.10	15.09 ± 0.10	14.30 ± 0.10
	4.06 ± 0.37	5.71 ± 0.53	6.00 ± 0.55	7.28 ± 0.67

Table 4: Fit parameters of homogeneous, one-zone SSC/EC models

	2200+420 1995	2200+420 1997	2200+420 Large	1749+096 1995	1749+096 Large	Notes
R	5×10^{15}	5×10^{15}	5×10^{17}	1×10^{15}	2×10^{18}	Radius of the emission region [cm]
ℓ_{in}	6.7×10^{-4}	1×10^{-2}	6×10^{-7}	8×10^{-3}	3×10^{-6}	Injected compactness
ℓ_{ex}	2×10^{-5}	2×10^{-3}	External compactness
γ_{max}	1.5×10^5	7×10^4	1.5×10^5	7×10^4	7×10^4	Maximum electron energy
γ_{peak}	1.3×10^3	1.3×10^3	1.5×10^3	5×10^2	5×10^2	Electron energy at ν_{peak}
s	2.7	2.8	2.5	3.1	3.1	Injected electron spectrum ($\propto \gamma^{-s}$)
B	0.73	0.73	2.6×10^{-3}	4.7	6.4×10^{-3}	Magnetic field [Gauss]
δ	15.5	15.5	15.5	14	14	Beaming factor
L_{ej}	1.3×10^{41}	2.6×10^{42}	1.1×10^{40}	3×10^{42}	2.2×10^{41}	Intrinsic electron power [erg s ⁻¹]